

Chair-like N_6^{6-} in AlN_3 with high-energy density

Shi-Tai Guo(郭世泰), Zhen-Zhen Xu(徐真真), Yan-Lei Geng(耿延雷), Qi Rui(芮琦), Dian-Chen Du(杜殿臣), Jian-Fu Li(李建福), and Xiao-Li Wang(王晓丽)
Citation: Chin. Phys. B, 2023, 32 (**12**): 126202. DOI: 10.1088/1674-1056/acfd1a
Journal homepage: http://cpb.iphy.ac.cn; http://iopscience.iop.org/cpb

What follows is a list of articles you may be interested in

Pressure induced insulator to metal transition in quantum spin liquid candidate $NaYbS_2$

Yating Jia(贾雅婷), Chunsheng Gong(龚春生), Zhiwen Li(李芷文), Yixuan Liu(刘以轩), Jianfa Zhao(赵建发), Zhe Wang(王哲), Hechang Lei(雷和畅), Runze Yu(于润泽), and Changqing Jin(靳常青)
Chin. Phys. B, 2023, 32 (**9**): 096201. DOI: 10.1088/1674-1056/accff0

New MgO-H_2O compounds at extreme conditions

Lanci Guo(郭兰慈) and Jurong Zhang(张车荣)
Chin. Phys. B, 2023, 32 (**7**): 076201. DOI: 10.1088/1674-1056/ace035

Pressure-induced structural transition and low-temperature recovery of sodium pentazolate

Zitong Zhao(赵梓彤), Ran Liu(刘然), Linlin Guo(郭琳琳), Shuang Liu(刘爽), Minghong Sui(隋明宏), Bo Liu(刘波), Zhen Yao(姚震), Peng Wang(王鹏), and Bingbing Liu(刘冰冰)
Chin. Phys. B, 2023, 32 (**4**): 046202. DOI: 10.1088/1674-1056/acb917

In situ study of calcite-III dimorphism using dynamic diamond anvil cell

Xia Zhao(赵霞), Sheng-Hua Mei(梅升华), Zhi Zheng(郑直), Yue Gao(高悦), Jiang-Zhi Chen(陈姜智), Yue-Gao Liu(刘月高), Jian-Guo Sun(孙建国), Yan Li(李艳), and Jian-Hui Sun(孙建辉)
Chin. Phys. B, 2022, 31 (**9**): 096201. DOI: 10.1088/1674-1056/ac6157

High-pressure study of topological semimetals XCd_2Sb_2 (X = Eu and Yb)

Chuchu Zhu(朱楚楚), Hao Su(苏豪), Erjian Cheng(程二建), Lin Guo(郭琳), Binglin Pan(泮炳霖), Yeyu Huang(黄烨煜), Jiamin Ni(倪佳敏), Yanfeng Guo(郭艳峰), Xiaofan Yang(杨小帆), and Shiyan Li(李世燕)
Chin. Phys. B, 2022, 31 (**7**): 076201. DOI: 10.1088/1674-1056/ac7212

RAPID COMMUNICATION

Chair-like N_6^{6-} in AlN_3 with high-energy density

Shi-Tai Guo(郭世泰)[1,2], Zhen-Zhen Xu(徐真真)[1], Yan-Lei Geng(耿延雷)[1], Qi Rui(芮琦)[2], Dian-Chen Du(杜殿臣)[2], Jian-Fu Li(李建福)[1,†], and Xiao-Li Wang(王晓丽)[2,‡]

[1] *School of Physics and Electronic Information, Yantai University, Yantai* 264005, *China*
[2] *School of Physics and Electronic Engineering, Linyi University, Linyi* 276005, *China*

(Received 26 July 2023; revised manuscript received 14 September 2023; accepted manuscript online 26 September 2023)

The search for stable novel polynitrogen clusters has garnered significant attention in the field of energetic materials due to their potential applications as high-energy-density materials. In this study, a chair-like N_6^{6-} ring with N–N single bonds in the AlN_3 compound is theoretically predicted through first-principles calculations in conjunction with an unbiased structure searching method. The predicted AlN_3 phase exhibits high kinetic and thermodynamic stability, along with a high energy density of 5.04 kJ/g relative to AlN and N_2 gas. Additionally, its detonation velocity and pressure are estimated to reach 12.93 km/s and 1009.63 kbar, respectively. These values are greater than those of TNT and HMX, positioning it as a promising candidate for high-energy-density materials in the field of explosive combustion. The analysis of electronic properties and the related chemical bonding patterns indicates that the compounds are stabilized by both Coulomb interactions and covalent bonds. More importantly, the calculated formation of enthalpy indicates that the N_6^{6-} anions within AlN_3 can be synthesized by compressing AlN and N_2 at a moderate pressure (46 GPa). These findings present a viable approach for synthesizing and stabilizing the all-nitrogen N_6^{6-} anions.

Keywords: high pressure, aluminum nitride, electronic property, high-energy-density materials

PACS: 62.50.–p, 82.40.Fp, 91.60.Gf **DOI:** 10.1088/1674-1056/acfd1a

1. Introduction

Recently, all-nitrogen salts have drawn much attention in the high-energy-density materials (HEDMs) field due to their potential as ideal candidates in propellant or explosive applications.[1] Generally, the high energy of these compounds is primarily attributed to the substantial disparity in bond energy between N–N or N=N bonds in nonmolecular nitrogen (160/418 kJ/mol) and the N≡N triple bond in N_2 molecule (954 kJ/mol). In the past decade, several nitrogen-rich metal compounds with high energy density have been reported, including Be–N,[2–6] Mg–N,[7,8] Al–N,[9–11] S–N,[12] Fe–N,[13–15] Cu–N,[16,17] Zn–N,[18–20] Se–N,[21] Hg–N,[22] Ta–N,[23] W–N,[24] Y–N,[25] Ne–N,[26] and others. Theoretical calculations and experimental synthesis have demonstrated the existence of diverse all-nitrogen ions or clusters ranging from N_3 to N_{13}.[27,28] However, the successful preparation of such compounds remains rare. In 2001, Christe's work demonstrated the stability of $N_5^+SbF_6^-$ and $N_5^+Sb_2F_{11}^-$ salts up to 70 °C.[29] More recently, Lu's group achieved a breakthrough in the field by experimentally synthesizing cyclo-N_5^-.[30,31] The achievement opens up new possibilities for further advancements in the field, particularly in the areas of explosives and propellants. As we all know, one notable example of a high-energy-density compound is cubic gauche nitrogen (cg-N), which is solely connected by N–N bonds and possesses a high energy density of 9.7 kJ/g – twice that of traditional energetic compounds like TNT and HMX. However, the synthesis of cg-N requires extremely high pressures and temperatures (2000 K, 110 GPa) conditions.[32] Finding high-energy-density single-bond poly-nitrogen compounds that can remain stable at lower pressures is a challenging task that requires a specific solution approach. Fortunately, the discovery of t-N,[33] a dynamically and mechanically stable compound at ambient pressure with an estimated energy density of approximately 11.31 kJ/g, encourages further exploration of high-energy-density materials within poly-nitrogen compounds under ambient conditions. This successful theoretical prediction was made in 2018, prompting researchers to continue the search for other potential candidates with similar properties. More recently, it has been observed that cg-N can exhibit stability in an acidic condition or when the surface is saturated with less electronegative adsorbates.[34]

Numerous planar or quasiplanar cyclo-N_6 anions have been predicted in Li, Mg, Ca, and Ba nitrides under high pressure.[7,35–37] However, they have not paid close attention to the microstructural characteristics of these cyclo-N_6 anions. It's worth noting that an in-plane distortion may occur in the cyclo-N_6 sub-lattices when the neutral π-aromatic system transforms into a charged anion. For instance, chair-like N_6 anions have been predicted in h-WN_6, TeN_6, and GdN_6,[38–40] where strong chemical bonding and charge transfers are believed to contribute to the structural stability. The synthesis of

†Corresponding author. E-mail: jianfuli@ytu.edu.cn
‡Corresponding author. E-mail: xlwang@ytu.edu.cn

© 2023 Chinese Physical Society and IOP Publishing Ltd

WN_6, as mentioned in Ref. [24], has led to an increased interest in the study of N_6 anions. However, it is important to note that the content of nitrogen in these compounds will be decreased, resulting in relatively lower energy density due to the larger molar mass of tungsten (W) and tellurium (Te). In a separate study conducted by Liu *et al.*,[41] they reported the existence of GaN_5 and GaN_6 compounds with high nitrogen contents. It is worth mentioning that gallium (Ga) and aluminum (Al) are elements belonging to the same group. Generally, aluminum has a small atomic radius, high valence electron density, and high electronegativity, which makes it capable of forming strong covalent bonds with nitrogen atoms. Meanwhile, the relatively lower molar mass of aluminum compared to Te, W, Gd, and Ga allows for higher nitrogen content in aluminum-based compounds. Moreover, Cui *et al*. have predicted the existence of a notable monoclinic phase with polymeric nitrogen chains ($P2_1/c$-AlN_3) for AlN_3.[9] This phase is stable within a specific pressure range of 43–85 GPa, which indicates that aluminum and nitrogen can indeed form nitrogen-rich compounds under high pressure. Based on these factors, it is reasonable to consider binary Al–N compounds as potential candidates for the search of N_6 anions.

In the present study, the R-3m-AlN_3 phase has been successfully designed, featuring a chair-like N_6^{6-} ring with N–N single bonds. The phonon dispersion calculations and first-principles molecular dynamics (FPMD) simulations indicate that the compound exhibits good kinetics and thermodynamic stabilities. The calculated electronic properties and chemical bonding patterns of R-3m-AlN_3 reveal that its high stability arises from a combination of Coulomb interactions and covalent bonds. These factors contribute to the compound's structural integrity and overall stability. Furthermore, the study calculates the formation of enthalpy for R-3m-AlN_3, suggesting that the compound can be synthesized by condensing AlN and N_2 under appropriate pressure.

2. Computational details

The structure prediction for the Al–N system was carried out using the particle swarm optimization (PSO) methodology implemented in the CALYPSO code.[42,43] This approach does not rely on any known structural information and has been successfully validated in various systems under high pressure, including binary and ternary systems.[44–50] For the structural optimization and electronic properties calculations, density functional theory (DFT) with the Perdew–Burke–Ernzerhof (PBE) exchange–correlation functional and generalized gradient approximation (GGA) was employed.[51] These calculations were performed utilizing the VASP code.[52] The all-electron projector augmented wave (PAW)[53] method was adopted to represent the ionic potentials, the valence electrons of Al and N atoms are $3s^23p^1$ and $2s^22p^3$, respectively. The plane-wave basis set cutoff (700 eV) and appropriate Monkhorst–Pack k-meshes[54] ($2\pi \times 0.03$ Å^{-1}) were used to ensure all enthalpy calculations converged less than 1 meV/atom. In addition, phonon dispersion curves were computed using the supercell method implemented in the PHONOPY code[55] to determine the dynamical stability. FPMD simulations were performed in the NVT ensemble from 300 K to 700 K through the Nosé–Hoover method[56,57] to assess the thermodynamic stability of the system at different temperatures. We calculated the elastic constants employing the strain–stress method[58] as adopted in the VASP code. Relative elastic property parameters were determined using the Voigt–Reuss–Hill approximations.[59] The chemical bonding mode of AlN_3 was executed by the solid state adaptive natural density partitioning (SSAdNDP) method.[60] Orbital calculations were carried out at the B3LYP/6-311+g(d) level of theory using the Gaussian 09 code.[61] Bader analysis[62] was utilized to determine the transfer of charge within the system. The crystal structure patterns were visualized through VESTA[63] software.

3. Results and discussion

3.1. Crystal structure

We conducted a comprehensive search for all potential structures within the AlN_3 system across a pressure range from 0 to 100 GPa. Subsequently, we identified a crystal structure that features an N_6 ring and proceeded to optimize these structures. The total energy of structures containing N_6 rings was calculated under ambient conditions. The results indicated that the structure with the R-3m space group exhibited the lowest energy among all the selected structures at 0 GPa, as shown in Fig. 1(a). Furthermore, it was observed that structures with chair and boat N_6 rings generally had lower energies compared to structures with planar N_6 rings in AlN_3. Simultaneously, the energy of structures with chair N_6 rings was generally lower than that with boat N_6 rings. This disparity arises since the bond angles between nitrogen atoms in chair N_6 rings tend to align more closely with the ideal angle (120°) in contrast to boat N_6 rings. This alignment reduction minimizes the electron cloud overlap and Coulomb repulsion, consequently elevating the energy level of the conformation. Additionally, a comparison was made between the energy of $P2_1/c$ -AlN_3 and R-3m-AlN_3 in the pressure range from 0 to 100 GPa (Fig. S1). The findings revealed that the $P2_1/c$ structure had lower energy compared to the R-3m structure. However, recent high-pressure experiments have encouraged us to continue the research on R-3m-AlN_3. It is worth noting that the recently synthesized bp-N is not the lowest in energy,[64,65] and materials like silicon and ice can form different phases under varying pressure–temperature paths.[66,67] This suggests that the phases with higher energy can be formed by controlling the synthesis conditions.

Table 1. Calculated structural parameter for *R*-3*m*-AlN_3 structure at 0 GPa.

Space group	Lattice parameters		Wyckoff position	Atomic coordinates (fractional)
R-3*m*	$a = b = 5.504$ Å	$\gamma = \beta = 90°$	6*c*	Al(0.333,0.667,0.406)
	$c = 7.594$ Å	$\gamma = 120°$	18*h*	N(0.858,0.142,0.959)

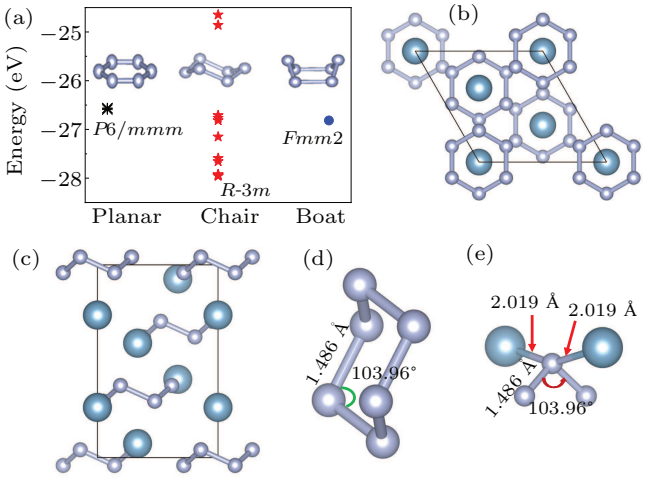


Fig. 1. Crystal structure of AlN_3. (a) Energy of AlN_3 with planar, chair, and boat N_6 rings units. (b) and (c) The structure of *R*-3*m*-AlN_3 phase. (d) Separate chaired N_6 ring structure. (e) The structural unit of 4-fold bonded N. Light blue and gray spheres represent Al and N atoms, respectively.

The *R*-3*m*-AlN_3 phase (Figs. 1(b) and 1(c)) and the separate chaired N_6 ring structure (Fig. 1(d)) are illustrated. Under atmospheric conditions, the bond length and bond angle for the chaired N_6 ring structure are equal, measuring 1.486 Å and 103.96°, respectively. In the *R*-3*m*-AlN_3 phase, six N atoms form an N_6 ring network, and each Al atom is bonded to six N atoms, forming an octahedral structure with a sixfold coordinated mode. Each N atom is driven by the sp^3 hybridization of two adjacent N atoms and Al atoms, forming four covalent bonds. The Al–N distances in the structure are 2.019 Å and 2.149 Å, respectively (Fig. 1(e)). The detailed information on the structure is summarized in Table 1.

3.2. Kinetic and thermal stability

To assess the kinetics stability of the *R*-3*m*-AlN_3 structure at 0 GPa, phonon spectra were computed using the supercell method. In general, the presence of imaginary frequencies in the phonon spectra typically suggests the potential for vibration mode instability. Conversely, the absence of imaginary frequencies indicates a lack of vibration modes that could lead to structural instability. This also implies that the structure remains stable across a range of vibration modes. As shown in Figs. 2(a) and 2(b), the absence of imaginary frequency in the over Brillouin zone demonstrates that the structure is kinetically stable. Based on the analysis of phonon density of states (PHDOS) for the *R*-3*m*-AlN_3 structure, it was observed that there are strongly coupled vibrations between the Al and N atoms, which contribute to the low-frequency vibration modes. Furthermore, the stretching mode of the N–N bond induces high-frequency vibrations.

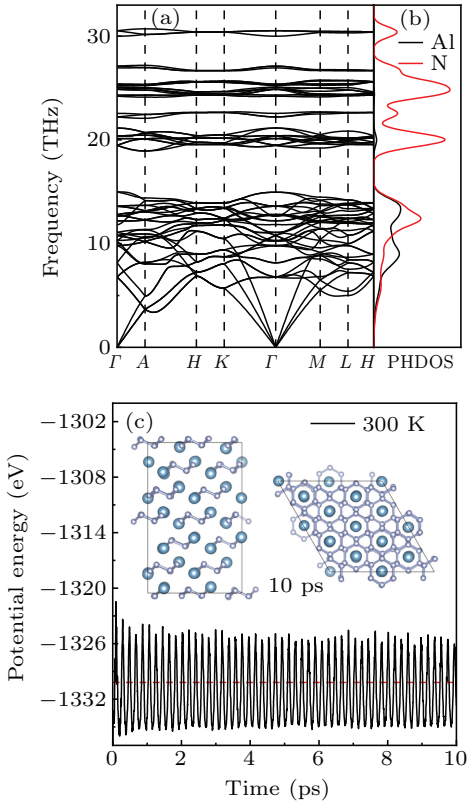


Fig. 2. The dynamical and thermodynamic stabilities of the *R*-3*m*-AlN_3 structure. (a) and (b) Phonon spectra and phonon DOS, respectively. (c) Fluctuations of the total energy of *R*-3*m* structure at the temperature of 300 K during FPMD simulations. The inset shows the structure pictures after 10 ps simulations at 300 K.

Similarly, the thermal stability of the N_6^{6-} anion in the *R*-3*m*-AlN_3 structure was assessed using a 2×2×2 supercell with 192 nitrogen atoms in the model. The evaluation was conducted through FPMD simulations, which were performed at a temperature of 300 K for 10 ps with a time step of 1 fs. The duration of 10 ps was chosen primarily because it allows for the observation of significant dynamic changes in the initial stage, such as structural changes and energy fluctuations, while also ensuring that the computational costs remain manageable. In Fig. 2(c), the potential energy of the analog system is observed to fluctuate around 1330.2 eV. The inset shows the picture of the equilibrium structure at the end of 10 ps simulations, demonstrating that the N_6^{6-} anion remains intact and is not broken, except for some thermal fluctuations. To further assess the thermal and kinetic stabilities, additional simulations were performed at higher temperatures. Figures S2 and S3 depict the temperature profiles at 500 K and 700 K, using a 1 fs time step. It is discovered that the N–N bond is broken at the 700 K temperature, leading to the disruption of the integrity of the N_6 ring. The plots of radial distribution function (RDF) for N–N separations are shown in Figs. S4 and S5.

The first sharp peak in the RDF represents the nearest distance between the selected atom and its nearest neighboring atoms. It is shown that there is a single RDF peak at approximately 1.488 Å corresponding to the N–N distance without significant change at 300 K and 500 K, which supports the conclusion that the R-3m-AlN_3 with N_6^{6-} remains stable at ambient conditions and high temperatures.

3.3. Mechanical stability

It is widely known that the mechanical properties of any crystal are strongly influenced by its fundamental elastic constants (C_{ij}). To verify the mechanical properties of the R-3m-AlN_3 structure at 0 GPa, the elastic constants were calculated using the strain–stress method.[58] The R-3m phase requires the determination of six independent elastic constants, and the Born–Huang criterion[68] was employed to verify the mechanical stability of the R-3m-AlN_3 structure at 0 GPa. The mechanical stability criteria for the hexagonal phase are evaluated based on the following conditions: $C_{44} > 0$, $zC_{11} > |C_{12}|$ $(C_{11}+2C_{12})C_{33} > 2C_{13}^2$. Obviously, the elastic constants of the structure satisfy these criteria, indicating its mechanical stability. Through the elastic constants, the corresponding shear modulus (G), bulk modulus (B), Young's modulus (E), and Poisson's ratio (ν) can be deduced by the Voigte–Reusse–Hill approximation,[59] as shown in Table 2.

Table 2. Calculated elastic constants C_{ij}, bulk modulus B, shear modulus G, Young's modulus E, and Poisson's ratio ν of R-3m-AlN_3 structure at ambient pressure.

	C_{11}	C_{12}	C_{13}	C_{33}	C_{44}	C_{66}	B (GPa)	G (GPa)	E (GPa)	ν
R-3m-AlN_3	447	117	97	233	165	124	185	133	322	0.21

It can be seen from Table 2, that the R-3m-AlN_3 phase exhibits a shear modulus of 133 GPa and a bulk modulus of 185 GPa. The Pugh criterion serves as an empirical approach used to predict the brittle or ductile behavior of crystalline materials. Importantly, it has been successfully applied to anticipate various material-related characteristics, and the outcomes of its predictions have gained recognition within the scientific community. According to Pugh's criterion,[69] the ratio of $k = G/B$ determines whether the materials behave in a brittle or ductile manner. If $k > 0.57$, the material behaves in a brittle manner; otherwise, it is ductile. In the case of R-3m-AlN_3, the calculated value of G/B (0.72) is larger than 0.57, similar to the diamond (1.10) and c-BN (0.86),[70] meaning the brittle materials. Additionally, the stiffness of a material can be characterized by Young's modulus,[71] the high value (322 GPa) indicates that the R-3m-AlN_3 structure can be used as a potential hard material. Poisson's ratio reflects the degree of covalent bonding in a material.[72] The value (0.21) is lower than 0.33, indicating a strong degree of covalent bonding. Taken together, these excellent mechanical parameters demonstrate the good mechanical stability of the R-3m-AlN_3 structure.

3.4. Electronic properties

The electronic band structure and projected density of states (PDOS) of the R-3m-AlN_3 phase at 0 GPa were calculated to explore its inner nature and formation mechanism, as shown in Fig. 3. The calculations reveal that the R-3m-AlN_3 structure possesses semiconductor property with a large band gap of 4.14 eV. This suggests its potential for applications in electronic devices and optoelectronics. However, density functional calculations usually lead to a significant underestimation of the energy gap due to several primary factors, such as the approximation of exchange–correlation functionals, self-interaction errors, the size of the basis set, etc. Therefore, the actual band gap is expected to be greater than 4.14 eV. In addition, the electronic band structure shows a clear overlap between the Al 3p and N 2p orbitals, demonstrating the formation of a strong chemical bonding as depicted in Figs. 3(b) and 3(c). To gain further insights into the behavior of the chemical bonds, Bader[62] charge analysis (shown in Table S1) was performed. The analysis revealed that there is a significant electron transfer (2.4e) between aluminum and nitrogen atoms. This information provides insights into the behavior of chemical bonds within the R-3m-AlN_3 structure.

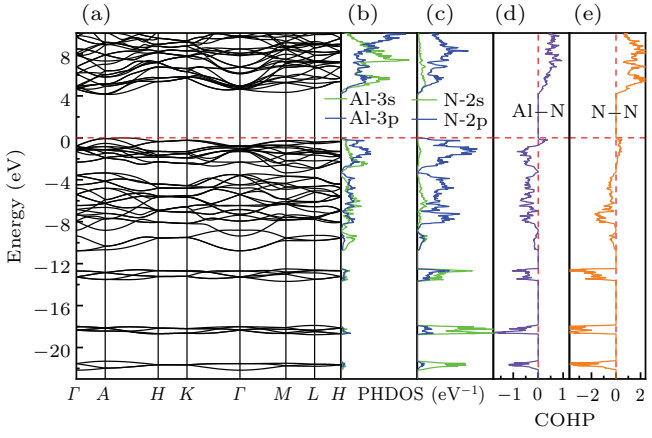


Fig. 3. Electronic properties of the R-3m structure of AlN_3. (a) Band structure. (b) and (c) Partial densities of states (PDOS) for Al and N, respectively. (d) and (e) The COHP between Al and N atoms and between N atoms, respectively.

The crystal orbital Hamiltonian group (COHP) is a target of energy resolution to measure the overlap strength and crystal orbital overlap population, which helps to understand the contribution of atomic pairs to the structural stability determining the bonding information based on the COHP in the LOBSTER program.[73] Generally speaking, the positive and negative COHP values indicate the presence of antibonding

and bonding states, respectively. The COHP plot of the Al–N pairs and N–N pairs are shown in Figs. 3(d) and 3(e), respectively. It is obvious that bonding states are fully occupied, and the antibonding states are not occupied, which demonstrates the strong covalent bond feature between them. In addition, the ICOHP values quantify the strength of the antibonding interaction. In this case, the ICOHP values corresponding to Figs. 3(d) and 3(e) are −4.49 and −9.18, respectively. These results reflect the strong covalent bonding characteristics between Al and N atoms in the Al–N pairs and the strong covalent bonding between neighboring N atoms in the N–N pairs.

3.5. Chemical bonding pattern

To illustrate the reason for the high stability of the *R*-3*m*-AlN_3 phase, the SSAdNDP method was used to analyze its chemical bonding patterns, relative results of the analysis are plotted in Fig. 4. In the primitive cell, there are 36 2*c*-2*e* Al–N σ bonds (Fig. 4(a)) and 18 2*c*-2*e* N–N σ bonds (Fig. 4(c)), the total number of electrons involved in these bonds is 108, which is in complete agreement with the sum of outer valence electrons in the AlN_3 unit cell. It is worth noting that one unit cell comprises six AlN_3 formulas, with Al and N elements contributing $3s^2 3p^1$ and $2s^2 2p^3$, respectively. The reasonable occupation numbers of these bonds indicate that the computational results are reliable. Moreover, the bonding modes of Al–N and N–N in the *R*-3*m*-AlN_3 phase are illustrated in Figs. 4(b) and 4(d), respectively. For the N_6^{6-} anion, each Al atom is bonded to six N atoms, forming a twisted ring structure. The distance between adjacent N atoms in the ring is measured to be 1.486 Å, which is close to the typical N–N single bond distance of 1.45 Å.[74] Furthermore, the *R*-3*m*-AlN_3 phase exhibits strong covalent bonding between N atoms and between Al and N atoms. This is evident due to the isosurface value exceeding 0.75, along with the presence of lone pair electrons, as revealed by the calculated electron localization functions (ELF)[75] shown in Figs. 4(e) and S6.

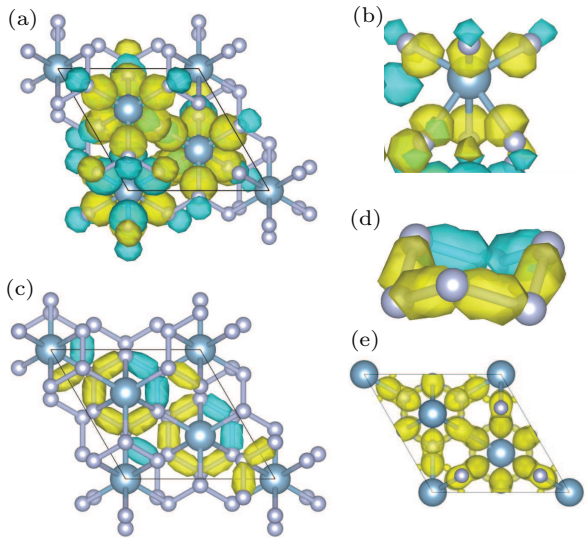


Fig. 4. Schematic of the SSAdNDP chemical bonding pattern for AlN_3 unit cell. (a) 36 2*c*-2*e* Al–N σ bonds, occupation number threshold: 1.75|*e*|, the isosurface value = 0.15. (c) 18 2*c*-2*e* N–N σ bonds, occupation number threshold: 1.75|*e*|, the isosurface value = 0.2. (b) and (d) The bonding modes of Al–N and N–N, respectively. (e) The calculated ELF, the isosurface value = 0.8.

To demonstrate the bonding situation, Fig. 5 displays a scheme of the molecular orbital diagram of the N_6^{6-}. The HOMO to HOMO-5 show that two p_z-like lone pair electrons occur at each atom of the N_6 molecule. The HOMO-6 to HOMO-11 show additional p_y-like lone pair electrons on each N atom. HOMO-12 to HOMO-17 show strong s–p σ bonds between N atoms. It is precise because the p_z lone pair electrons of N_6^{6-} enter the 3p orbital of the Al atom, leading to the formation of the coordinated covalent bond between the Al atom and the N atom.

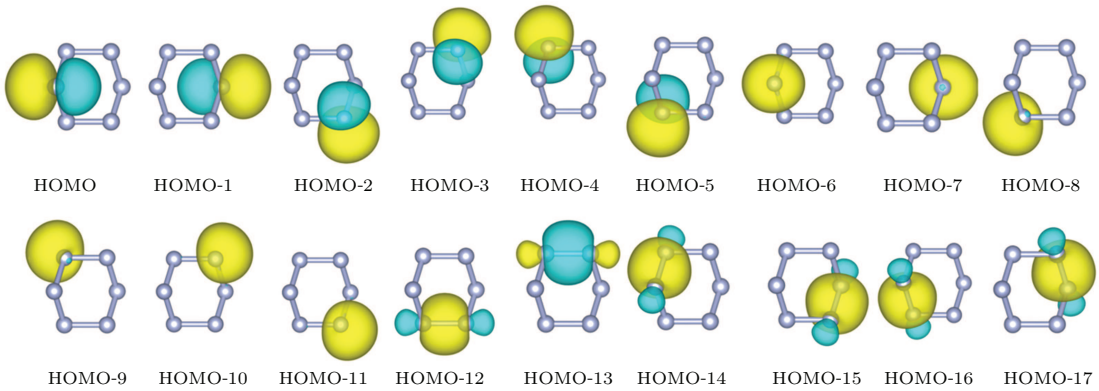


Fig. 5. Occupied orbitals of the N_6^{6-}. The isosurface value is ±0.05 and the blue and yellow colors denote negative and positive values, respectively.

3.6. Stabilization mechanism

Indeed, the presence of Al atoms significantly enhances the stability of N_6^{6-} anion in the AlN_3 structure due to two types of interactions between Al^{3+} and N_6^{6-}. Firstly, Coulomb interactions play a role in stabilizing the structure. Aluminum atoms in the AlN_3 structure lose their 3s and 3p electrons, resulting in the formation of Al^{3+} cations. Conversely, the N_6 gains six electrons, leading to the formation of N_6^{6-} an-

ions. Hence, Coulomb interactions between them are established. Secondly, covalent bonding between Al^{3+} and N_6^{6-} is observed in various calculations. These results demonstrate the presence of covalent bonding characteristics between Al^{3+} and N_6^{6-}. In short, the two mechanisms between Al^{3+} cations and N_6^{6-} anions work together for the high structural stability of the AlN_3 structure.

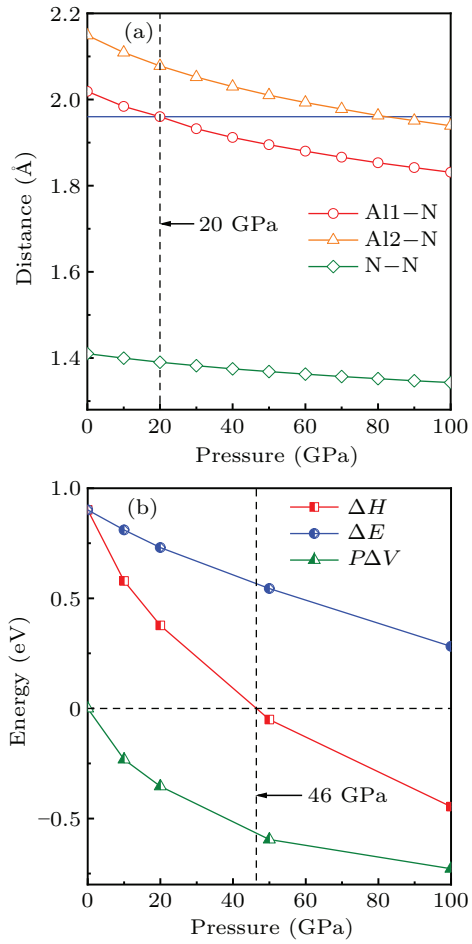


Fig. 6. Pressure-driven reaction mechanism between AlN with N_2. (a) The relationship between atomic distance and external pressure. The blue line represents the sum (1.96 Å) of Al-3p and N-2p covalent radii; the green line indicates the N–N distance for cg-N. (b) Calculated enthalpy difference (ΔH), internal energy (ΔE), and volume term ($P\Delta V$) with pressure for the formation of AlN_3. For the chemical reaction of AlN + N_2 → AlN_3, we defined $\Delta H = H_{AlN_3} - H_{AlN} - H_{N_2}$, $\Delta E = E_{AlN_3} - E_{AlN} - E_{N_2}$, $P\Delta V = PV_{AlN_3} - PV_{AlN} - PV_{N_2}$, where P and V represent the pressure and volume per formula unit, respectively.

Subsequently, we investigated the formation mechanism of Al–N covalent bonds by analyzing the relationship between Al–N distances and the ever-increasing pressure, as depicted in Fig. 6(a). Our calculations revealed that the distances between Al and N atoms gradually decrease as the pressure increases. Notably, the Al–N distance reaches the sum (1.96 Å) of the covalent radii[76] of Al 3p and N 2p at a pressure of 20 GPa. Moreover, it is worth mentioning that throughout the pressure range studied, the Al–N distance remains larger than the N–N distance in the case of cg-N. This result provides strong evidence supporting the covalent bonding nature of the Al–N bonds.

To illustrate the decomposition of AlN_3 into AlN and N_2 at high pressure, we plot the enthalpy difference (ΔH) between AlN_3 and AlN + N_2. Additionally, we analyze the contributions to ΔH from the internal energy (ΔE) and volume term ($P\Delta V$), as shown in Fig. 6(b). It reveals that the decomposition of AlN_3 into AlN and N_2 occurs spontaneously at pressures higher than 46 GPa. Furthermore, the competition between the ΔE and $P\Delta V$ terms is crucial in determining the actual chemical reaction. Although ΔE remains largely positive, the $P\Delta V$ term is negative due to the associated volume reduction, and this effect becomes more substantially reduced as the pressure increases. At 46 GPa, the $P\Delta V$ term dominates the competition, leading to a negative ΔH value and the formation of the stable AlN_3 compound.

3.7. Explosive performance

The energy density is a crucial parameter for evaluating the detonation properties of a material. Here, in the case of the predicted stable phase of R-3m-AlN_3, a significant amount of chemical energy is released when it dissociates into stable AlN solid and dinitrogen gas under ambient conditions. Considering the energy reduction of nitrogen gas concerning the α nitrogen phase (around 0.25 eV/atom),[80] the chemical energy densities (E_d) of dense R-3m-AlN_3 with a density of 3.45 g/cm^3 can be calculated to be approximately 5.04 kJ/g (Table 3). This calculation is based on the dissociation of AlN_3 (s) → AlN (s) + N_2 (g) and referencing to the energy of their most stable phase at 0 GPa.[81,82] Strikingly, the performance of R-3m-AlN_3 in terms of energy density surpasses that of the typical explosive material TNT (4.3 kJ/g).[77] Furthermore, the volumetric energy densities (E_v) of R-3m-AlN_3 are estimated to be 17.39 kJ/cm^3, which is approximately 2.5 times that of TNT (∼ 7.05 kJ/cm^3) and 1.6 times that of HMX (∼ 10.83 kJ/cm^3).

Table 3. Detonation properties of R-3m-AlN_3 estimated by Kamlet–Jacobs empirical equations, compared to the experimental values of the known explosives of TNT and HMX.[77–79]

Compounds	ρ (g/cm^3)	E_d (kJ/g)	E_v (kJ/cm^3)	V_d (km/s)	P_d (kbar)
R-3m-AlN_3	3.45	5.04	17.39	12.93	1009.63
TNT	1.64	4.30	7.05	6.90	190
HMX	1.90	5.70	10.83	9.10	393

The detonation properties of the R-3m-AlN_3 structure, including detonation velocities (V_d) and detonation pressures (P_d), are important indicators for evaluating its suitability as a HEDM.[83] The empirical Kamlet–Jacobs equations[79] provide a way to estimate V_d and P_d based on certain parameters. The equations for V_d and P_d are given as follows: $V_d = 1.01(NM^{0.5}E_d^{0.5})^{0.5}(1 + 1.3\rho)$ and $P_d = 15.58\rho^2 NM^{0.5}E_d^{0.5}$. Here, N represents the moles of dinitrogen gas per gram of AlN_3, M represents the molar mass (28 g/mol) of dinitrogen gas, and E_d is the chemical detonation energy expressed in

kJ/g. They have successfully predicted the experimental values of V_d and P_d for TNT (6.90 km/s, 190 kbar) and HMX (9.10 km/s, 393 kbar), respectively.[84] After simulating the empirical equations, the detonation velocity and detonation pressure of the R-3m-AlN_3 phase were estimated to be up to 12.93 km/s and 1009.63 kbar. These values are nearly 1.9 and 5.3 times higher than that of TNT, and approximately 1.4 and 2.5 times higher than that of HMX. These high detonation performances manifest the potential application of R-3m-AlN_3 in high explosives. It is worth noting that these values of traditional energetic materials (TNT, HMX, and CL-20) are typically measured under experimental conditions. In contrast, the performance parameters of the R-3m-AlN_3 phase are calculated using first-principles methods, without considering the energy consumption during experiments. Consequently, the actual performance parameters are likely to be lower than the calculated values. Nevertheless, these calculations still hold significant reference value.

3.8. Route to chair-like N_6^{6-} anion

In the conducted research, an experimental synthesis of aluminum nitride (AlN) in the $P6_3mc$ phase (wurtzite structure) has been successfully achieved and found to be stable within the pressure range of 0–20 GPa.[81] Here, to explore the feasibility of synthesizing R-3m-AlN_3 under high pressure, the formation enthalpy of AlN_3 relative to AlN and N_2 (Fig. 7) has been calculated. Additionally, the phase transition process of AlN and N is shown in Figs. S7 and S8, respectively. The result shows that the R-3m-AlN_3 exhibits lower energy compared to AlN and N_2 under pressures exceeding 46 GPa. This suggests that the synthesis of N_6^{6-} can be achieved by condensing AlN and N_2 at 46 GPa. Importantly, the structure remains mechanically stable under ambient conditions, which raises the possibility of recovery at ambient conditions.

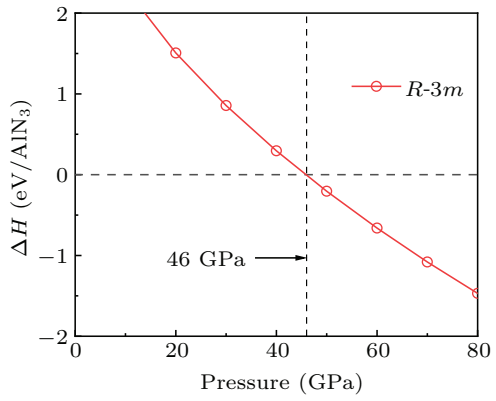


Fig. 7. Enthalpy of formation of R-3m-AlN_3 relative to AlN and N_2.

4. Conclusions

Through swarm-intelligence structure searches, the presence of all-nitrogen anions N_6^{6-} in the AlN_3 compound has been predicted. The calculation results of phonon dispersion and FPMD suggest that the R-3m-AlN_3 structure exhibits excellent kinetic and thermal stabilities at atmospheric pressure. Meanwhile, it demonstrates good mechanical stability at 0 GPa. The high stability of R-3m-AlN_3 is attributed to the combined effects of Coulomb interactions and covalent bonds between Al^{3+} and N_6^{6-}. Further analysis of the electronic properties reveals that the structure possesses a semiconductor character with a large band gap of 4.14 eV. In addition, the calculated formation enthalpies of R-3m-AlN_3 indicate that it can be synthesized by condensing AlN and N_2 under appropriate pressure conditions. Upon decomposition, AlN_3 releases a substantial amount of energy, with a calculated energy release of 5.04 kJ/g. This indicates it possesses outstanding detonation properties, including high detonation velocity and pressure. For instance, the detonation velocity and pressure are approximately 1.9 and 5.3 times higher than that of TNT. These characteristics position R-3m-AlN_3 as a promising candidate for high-energy-density material. The findings of this study are expected to facilitate the experimental synthesis of the AlN_3 phase and stimulate further research on all-nitrogen salts.

Acknowledgements

Project supported by the National Natural Science Foundation of China (Grant No. 11974154), the Taishan Scholars Special Funding for Construction Projects, and the Natural Science Foundation of Shandong Province (Grant No. ZR2022MA004).

References

[1] Talawar M B, Sivabalan R, Asthana S N and Singh H 2005 *Combust. Explos. Shock Waves* **41** 264
[2] Zhang S T, Zhao Z Y, Liu L L and Yang G C 2017 *J. Power Sources* **365** 155
[3] Li X Y, Zhang S H, Zhang C Z and Wang Q 2018 *Nanoscale* **10** 949
[4] Li J F, Jiang Q W, Zhu Z Q, Zhu H Y and Wang X L 2018 *Europhys. Lett.* **124** 67004
[5] Lin J N, Zhu Z Q, Jiang Q W, Guo S T, Li J F, Zhu H Y and Wang X L 2019 *AIP Adv.* **9** 055116
[6] Lin J N, Wang F X, Rui Q, Li J F, Wang Q L and Wang X L 2022 *Matter Radiat. Extrem.* **7** 038401
[7] Wei S L, Li D, Liu Z, Li X, Tian F B, Duan D F, Liu B B and Cui T 2017 *Phys. Chem. Chem. Phys.* **19** 9246
[8] Xia K, Zheng X X, Yuan J N, Liu C, Gao H, Wu Q and Sun J 2019 *J. Phys. Chem. C* **123** 10205
[9] Liu Z, Li D, Wei S L, Wang W J, Tian F B, Bao K, Duan D F, Yu H Y, Liu B B and Cui T 2017 *Inorg. Chem.* **56** 7494
[10] Liu Z, Li D, Liu Y, Cui T, Tian F B and Duan D F 2019 *Phys. Chem. Chem. Phys.* **21** 12029
[11] Du H F, Ge Y F, Zhu J L, Guo W and Yao Y G 2021 *Phys. Chem. Chem. Phys.* **23** 12350
[12] Li D, Tian F B, Lv Y Z, Wei S L, Duan D F, Liu B B and Cui T 2017 *J. Phys. Chem. C* **121** 1515
[13] Bykov M, Bykova E, Aprilis G, Glazyrin K, Koemets E, Chuvashova I, Kupenko I, McCammon C, Mezouar M, Prakapenka V, Liermann H P, Tasnádi F, Ponomareva A V, Abrikosov I A, Dubrovinskaia N and Dubrovinsky L 2018 *Nat. Commun.* **9** 2756

[14] Jiao F B, Zhang C Y and Xie W 2020 *J. Phys. Chem. C* **124** 19953
[15] Sun C L, Guo W and Yao Y G 2022 *Chin. Phys. Lett.* **39** 087101
[16] Li J F, Sun L, Wang X L, Zhu H Y and Miao M S 2018 *J. Phys. Chem. C* **122** 22339
[17] Yi W C, Zhao K F, Wang Z X, Yang B C, Liu Z and Liu X B 2020 *ACS Omega* **5** 6221
[18] Liu Z, Li D, Tian F B, Duan D F, Li H D and Cui T 2020 *Inorg. Chem.* **59** 8002
[19] Shi X H, Yao Z and Liu B B 2020 *J. Phys. Chem. C* **124** 4044
[20] Xin S S, Du D C, Wang F X, Rui Q, Wang Q L, Zhao X L, Li J F, Yang D J, Zhu H Y and Wang X L 2021 *Phys. B* **617** 413139
[21] Wang W J, Wang H, Liu Y, Li D, Tian F B, Duan D F, Yu H Y and Cui T 2019 *Inorg. Chem.* **58** 2397
[22] Guo S T, Lin J N, Li J F, Wang Q L, Wu H, Zhu H Y and Wang X L 2019 *Comput. Mater. Sci.* **169** 109147
[23] Xing W D, Wei Z J, Yu R and Meng F Y 2019 *J. Mater. Sci. Technol.* **35** 2297
[24] Salke N P, Xia K, Fu S Y, Zhang Y J, Greenberg E, Prakapenka V B, Liu J, Sun J and Lin J F 2021 *Phys. Rev. Lett.* **126** 065702
[25] Miao J Y, Lu Z S, Peng F and Lu C 2021 *Chin. Phys. Lett.* **38** 066201
[26] Liu L L, Zhang S T and Zhang H J 2022 *Chin. Phys. Lett.* **39** 056102
[27] Peng F, Yao Y S, Liu H Y and Ma Y M 2015 *J. Phys. Chem. Lett.* **6** 2363
[28] Kulkarni A, Schön J C, Doll K and Jansen M 2013 *Chem. - An Asian J.* **8** 743
[29] Vij A, Wilson W W, Vij V, Tham F S, Sheehy J A and Christe K O 2001 *J. Am. Chem. Soc.* **123** 6308
[30] Zhang C, Sun C G, Hu B C, Yu C M and Lu M 2017 *Science* **355** 374
[31] Xu Y G, Wang Q, Shen C, Lin Q H, Wang P C and Lu M 2017 *Nature* **549** 78
[32] Eremets M I, Gavriliuk A G, Trojan I A, Dzivenko D A and Boehler R 2004 *Nat. Mater.* **3** 558
[33] Li Y W, Feng X L, Liu H Y, Hao J, Redfern S A T, Lei W W, Liu D and Ma Y 2018 *Nat. Commun.* **9** 722
[34] Chen G, Niu C P, Xia W M, Zhang J, Zeng Z and Wang X L 2023 *Chin. Phys. Lett.* **40** 086102
[35] Prasad D L V K, Ashcroft N W and Hoffmann R 2013 *J. Phys. Chem. C* **117** 20838
[36] Zhu S S, Peng F, Liu H Y, Majumdar A, Gao T and Yao Y S 2016 *Inorg. Chem.* **55** 7550
[37] Huang B W and Frapper G 2018 *Chem. Mater.* **30** 7623
[38] Xia K, Gao H, Liu C, Yuan J N, Sun J, Wang H T and Xing D Y 2018 *Sci. Bull.* **63** 817
[39] Liu Z, Li D, Zhuang Q, Tian F B, Duan D F, Li F F and Cui T 2020 *Commun. Chem.* **3** 42
[40] Liu L L, Wang D H, Zhang S Z and Zhang H J 2021 *J. Mater. Chem. A* **9** 16751
[41] Liu Z, Li D, Wei S L, Liu Y, Tian F B, Duan D F and Cui T 2019 *Phys. Lett. A* **383** 125859
[42] Wang Y C, Lv J, Zhu L and Ma Y M 2012 *Comput. Phys. Commun.* **183** 2063
[43] Wang Y C, Lv J, Zhu L and Ma Y M 2010 *Phys. Rev. B* **82** 094116
[44] Peng F, Song X Q, Liu C, Li Q, Miao M S, Chen C F and Ma Y M 2020 *Nat. Commun.* **11** 5227
[45] Lu W C, Liu S Y, Liu G T, Hao K, Zhou M, Gao P Y, Wang H B, Lv J, Gou H Y, Yang G C, Wang Y C and Ma Y M 2022 *Phys. Rev. Lett.* **128** 106001
[46] Liu Y, Wang R, Wang Z G, Li D and Cui T 2022 *Nat. Commun.* **13** 412
[47] Lin J Y, Du X, Rahm M, Yu H, Xu H Y and Yang G C 2020 *Angew. Chem. Int. Ed.* **59** 9155
[48] Shi J M, Cui W W, Hao J, Xu M L, Wang X L and Li Y W 2020 *Nat. Commun.* **11** 3164
[49] Huang P H, Liu H Y, Lv J, Li Q, Long C H, Wang Y C, Chen C F, Hemley R J and Ma Y M 2020 *Proc. Natl. Acad. Sci. USA* **117** 5638
[50] Li X, Huang X L, Duan D F, Pickard C J, Zhou D, Xie H, Zhuang Q, Huang Y P, Zhou Q, Liu B B and Cui T 2019 *Nat. Commun.* **10** 3461
[51] Perdew J P, Burke K and Ernzerhof M 1996 *Phys. Rev. Lett.* **77** 3865
[52] Kresse G and Furthmüller J 1996 *Phys. Rev. B* **54** 11169
[53] Blöchl P E 1994 *Phys. Rev. B* **50** 17953
[54] Monkhorst H J and Pack J D 1976 *Phys. Rev. B* **13** 5188
[55] Dabhi S D and Jha P K 2015 *Polymer.* **81** 45
[56] Hoover W G 1985 *Phys. Rev. A* **31** 1695
[57] Nosé S 1984 *J. Chem. Phys.* **81** 511
[58] Le Page Y and Saxe P 2002 *Phys. Rev. B* **65** 104104
[59] Watt J P and Peselnick L 1980 *J. Appl. Phys.* **51** 1525
[60] Galeev T R, Dunnington B D, Schmidt J R and Boldyrev A I 2013 *Phys. Chem. Chem. Phys.* **15** 5022
[61] Frisch M J, Trucks G W, and Schlegel H B 2009 Gaussian 09. Gaussian Inc, Wallingford CT
[62] Tang W, Sanville E and Henkelman G 2009 *J. Phys. Condens. Matter* **21** 084204
[63] Momma K and Izumi F 2011 *J. Appl. Crystallogr.* **44** 1272
[64] Laniel D, Winkler B, Fedotenko T, Pakhomova A, Chariton S, Milman V, Prakapenka V, Dubrovinsky L and Dubrovinskaia N 2020 *Phys. Rev. Lett.* **124** 216001
[65] Ji C, Adeleke A A, Yang L X, Wan B, Gou H Y, Yao Y S, Li B, Meng Y, Smith J S, Prakapenka V B, Liu W J, Shen G Y, Mao W L and Mao H K 2020 *Sci. Adv.* **6** eaba9206
[66] Lin C L, Liu X Q, Yong X, Tse J S, Smith J S, English N J, Wang B H, Li M, Yang W G and Mao H K 2020 *Proc. Natl. Acad. Sci. USA* **117** 15437
[67] Lin C L, Liu X Q, Yang D L, Li X D, Smith J S, Wang B H, Dong H N, Li S R, Yang W G and Tse J S 2020 *Phys. Rev. Lett.* **125** 155702
[68] Wu Z J, Zhao E J, Xiang H P, Hao X F, Liu X and Meng J 2007 *Phys. Rev. B* **76** 054115
[69] Pugh S F 1954 *Philos. Mag.* **45** 823
[70] Tian F B, Wang J H, He Z, Ma Y M, Wang L C, Cui T, Chen C B, Liu B B and Zou G T 2008 *Phys. Rev. B* **78** 235431
[71] Kaner R B, Gilman J J and Tolbert S H 2005 *Science* **308** 1268
[72] Greaves G N, Greer A L, Lakes R S and Rouxel T 2011 *Nat. Mater.* **10** 823
[73] Maintz S, Deringer V L, Tchougréeff A L and Dronskowski R 2016 *J. Comput. Chem.* **37** 1030
[74] Morino Y, Iijima T and Murata Y 1960 *Bull. Chem. Soc. Jpn.* **33** 46
[75] Becke A D and Edgecombe K E 1990 *J. Chem. Phys.* **92** 5397
[76] Cordero B, Gómez V, Platero-Prats A E, Revés M, Echeverría J, Cremades E, Barragán F and Alvarez S 2008 *Dalton. Trans.* **21** 2832
[77] Hu Y, Huang P, Guo L, Wang X H and Zhang C L 2006 *Phys. Lett. A* **359** 728
[78] Kamlet M J and Jacobs S J 1968 *J. Chem. Phys.* **48** 23
[79] Kamlet M J and Dickinson C 1968 *J. Chem. Phys.* **48** 43
[80] Zhang J, Oganov A R, Li X F and Niu H Y 2017 *Phys. Rev. B* **95** 020103
[81] Xia Q, Xia H and Ruoff A L 1993 *J. Appl. Phys.* **73** 8198
[82] Pickard C J and Needs R J 2009 *Phys. Rev. Lett.* **102** 125702
[83] Geith J, Klapötke T M, Weigand J and Holl G 2004 *Propellants, Explos. Pyrotech.* **29** 3
[84] Wang Y, Liu Y L, Song S W, Yang Z J, Qi X J, Wang K C, Zhang Q H and Tian Y 2018 *Nat. Commun.* **9** 2444